Neutron diffraction studies on the multiferroic conical magnet Ba$_2$Mg$_2$Fe$_{12}$O$_{22}$

Shintaro Ishiwata,[1,2,][*] Daisuke Okuyama,[1] Kazuhisa Kakurai,[3] Masakazu Nishi,[4] Yasujiro Taguchi,[1] and Yoshinori Tokura[1,2,5]

[1]*Cross-Correlated Materials Research Group (CMRG) and Correlated Electron Research Group (CERG), RIKEN-ASI,*
Wako 351-0198, Japan

[2]*Department of Applied Physics and Quantum-Phase Electronics Center (QPEC), University of Tokyo, Hongo, Tokyo 113-8656, Japan*

[3]*Quantum Beam Science Directorate, Japan Atomic Energy Agency, Tokai, Ibaraki 319-1195, Japan*

[4]*Institute for Solid State Physics, University of Tokyo, Kashiwanoha, Kashiwa, Chiba 277-8581, Japan*

[5]*Multiferroics Project, ERATO, Japan Science and Technology Agency (JST), University of Tokyo, Tokyo 113-8656, Japan*

Magnetic structure of a multiferroic Y-type hexaferrite Ba$_2$Mg$_2$Fe$_{12}$O$_{22}$ with helical-spin structures propagating along [001] below 195 K has been extensively studied, using polarized and unpolarized neutron diffractions under transverse magnetic fields B ($\perp$[001]) up to 4.5 T. At zero magnetic field, a longitudinal-conical spin state was found to emerge below about 50 K, which enables the low-B control of electric polarization P. The magnetic phase diagram was investigated as a function of transverse B and coexistence of several phases with different helical-spin periodicity was confirmed at low-B region. Furthermore, by using the polarized neutron diffraction under transverse B, we verified that the ferroelectric phase with the largest P value with a commensurate $\boldsymbol{k}_0$ vector of (0, 0, 3/2) has a transverse-conical spin structure, in which the spin component perpendicular to B shows every 90° rotation with translation along the $\boldsymbol{k}_0$ direction. The relation between the transverse-conical spin structure and P as a function of the transverse B was discussed in terms of the inverse Dzyaloshinskii-Moriya model.

PACS number(s): 75.25.−j, 75.85.+t, 75.50.−y

I. INTRODUCTION

Discovery of magnetically controllable ferroelectricity induced by a cycloidal spin order has developed a new class of magnetoelectric (ME) materials.[1–8] While the progress in this class of materials toward applications has been hampered by the limitation of the available temperature or magnetic-field ranges, Y-type hexaferrites with a proper-screw spin order, such as Ba$_{0.5}$Sr$_{1.5}$Zn$_2$Fe$_{12}$O$_{22}$ and Ba$_2$Mg$_2$Fe$_{12}$O$_{22}$, have drawn considerable attention for their exceptionally high magnetic ordering temperatures.[9–13] Although both hexaferrites are paraelectric in the absence of external magnetic fields B, application of the transverse B perpendicular to the propagation vector $\boldsymbol{k}_0$ along the hexagonal axis [001] yields electric polarization P. In addition, the direction and the magnitude of P of Ba$_2$Mg$_2$Fe$_{12}$O$_{22}$ can be easily controlled by B of a few tens of milliteslas.[10,11]

It has been proposed that noncollinearly aligned, neighboring spins $\boldsymbol{s}_i$ and $\boldsymbol{s}_j$ produce an electric polarization $\boldsymbol{p}$ expressed as $\boldsymbol{p} = A\boldsymbol{e}_0 \times (\boldsymbol{s}_i \times \boldsymbol{s}_j)$ ($\boldsymbol{e}_0 = \boldsymbol{k}_0/|\boldsymbol{k}_0|$), which is so-called the spin-current model or the inverse Dzyaloshinskii-Moriya (DM) model.[14–17] The constant A depends mainly on the spin-orbit interaction and the exchange interaction. Thus, the cycloidal or transverse-conical spin structures are expected to generate P perpendicular to both $\boldsymbol{k}_0$ and the screw axis (parallel to the vector sum of $\Sigma \boldsymbol{s}_i \times \boldsymbol{s}_j$), whereas the proper screw and the longitudinal-conical spin structures are not. According to the theoretical phase diagram proposed by Nagamiya,[18] the proper-screw spin structure transforms into fan-type structure upon the application of transverse B ($\perp \boldsymbol{k}_0$), when the planar magnetic anisotropy is dominant over the superexchange interactions. However, when the planar magnetic anisotropy becomes less effective, the transverse-conical spin state with a finite P is allowed by the

application of even quite low B. Therefore, in the proper-screw spin system, the weak magnetic anisotropy is one of the important criteria for the realization of magnetically controllable multiferroicity. A cubic spinel compound ZnCr$_2$Se$_4$ (Ref. 19) and a Y-type hexaferrite Ba$_2$Mg$_2$Fe$_{12}$O$_{22}$ (Refs. 10 and 11) are examples of those which satisfy this criterion. In fact, a systematic study of the ME properties of Ba$_2$(Mg$_{1−x}$Zn$_x$)$_2$Fe$_{12}$O$_{22}$ with controlled anisotropy has revealed that the enhancement of the planar magnetic anisotropy strongly suppressed the B-induced ferroelectricity with destabilizing the conical spin structure at zero field.[20] The importance of the magnetic anisotropy for the multiferroic properties of Y-type hexaferrites was also discussed in Ref. 13.

The spins in Ba$_2$Mg$_2$Fe$_{12}$O$_{22}$ are known to be ferrimagnetically ordered within two kinds of blocks (L and S) with lying on the (001) plane, which allows us to describe the ordered states in terms of the alternate stacking of large magnetic moments (L spin) at the L blocks and the smaller moments (S spins) at the S blocks, as illustrated in Fig. 1. Based on neutron diffraction studies, this material was found to be collinear-spin ferrimagnetic below 553 K and proper screw below 195 K at $B=0$ (Refs. 21–23). Furthermore, magnetization measurements have indicated a possibility of a transition to the longitudinal-conical spin state below about 50 K, whose ferromagnetic moment endows this material with the low-B control of P (Ref. 10). Quite recently, Kida *et al.* reported the observation of electric-dipole active magnetic excitations, called electromagnons, at terahertz frequencies in this longitudinal-conical spin state and found the gigantic change in the intensity of the absorption by applying low B of less than 0.2 T along [001].[24]

Considering the inverse DM model and the experimental fact that the observed P is perpendicular to both $\boldsymbol{k}_0$ and B, it is natural to presume that the transverse-conical spin struc-
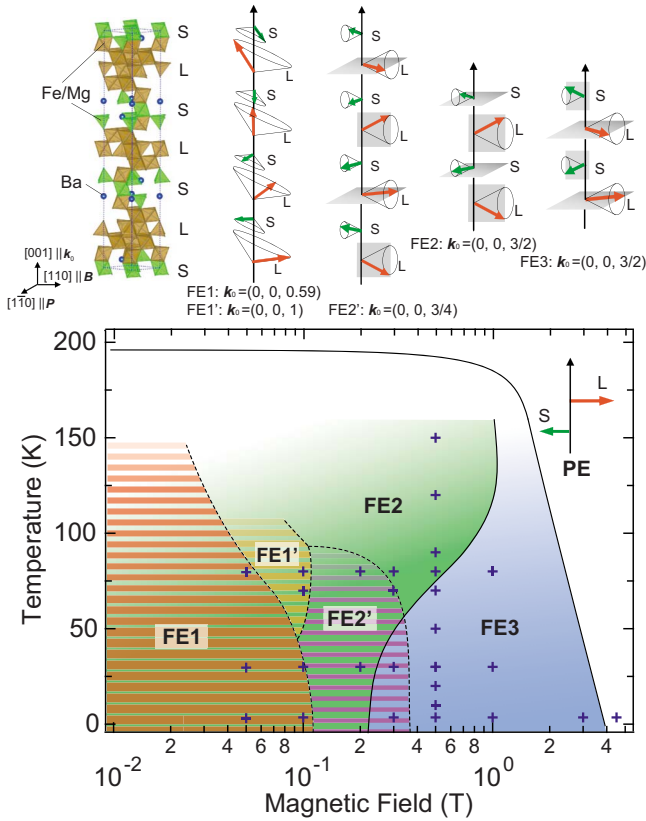
FIG. 1. (Color online) In the lower panel, a magnetic phase diagram of $Ba_2Mg_2Fe_{12}O_{22}$ is shown (FE and PE denote ferroelectric and paraelectric phases, respectively). The phase coexistence at low temperatures and low magnetic fields is represented by the stripes. Cross symbols denote the points at which neutron diffraction data were collected. The crystal structure of $Ba_2Mg_2Fe_{12}O_{22}$ and the schematic magnetic structure of each phase are shown in the upper panel. L and S stand for two kinds of magnetic sublattices with large and small magnetic moments. Each phase except for FE1 is characterized by the commensurate value of δ.

ture, whose screw axis is parallel to B, is the most appropriate model for the B-induced ferroelectric phase in $Ba_2Mg_2Fe_{12}O_{22}$ with a helimagnetic ground state. In the previous works, both from the ME and the magnetic measurements, the ME phase diagram and possible magnetic structures under transverse B were proposed.[10,20] Recently, the magnetic phase diagram of $Ba_2Mg_2Fe_{12}O_{22}$ up to B of 0.5 T, containing several phases with different periodicities, has been reported by neutron diffraction experiments with adopting a scattering vector $\boldsymbol{Q}$ of $(1, 0, l)$.[25] However, the magnetic structures and the origin of the B-induced ferroelectricity in $Ba_2Mg_2Fe_{12}O_{22}$ have remained unclear due to the lack of information other than the magnetic propagation vector. In this paper, by neutron diffraction experiments with the use of a pair of scattering vectors being orthogonal with each other, we identified a longitudinal-conical spin state below about 50 K in the absence of B and also investigated the magnetic structures of $Ba_2Mg_2Fe_{12}O_{22}$ under transverse B. Furthermore, by using the polarized neutron diffraction under the transverse B up to 4.5 T, we verified that the ferroelectric phase with the largest P (see the FE3 in Fig. 1) has a

transverse-conical spin structure whose projection onto a plane perpendicular to B consists of rotating spins by 90° with respect to the adjacent spins. On these bases, the relation between the transverse-conical spin structure and P will be discussed in terms of the inverse DM model.

II. EXPERIMENT

Single crystalline samples of $Ba_2Mg_2Fe_{12}O_{22}$ were grown by a flux method as described in Ref. 23. Magnetic properties were measured with a superconducting quantum interference device magnetometer. The unpolarized and polarized neutron diffraction measurements were performed using the triple-axis spectrometer TAS-1 installed at the JRR-3 of Japan Atomic Energy Agency in Tokai, Japan.[26] The lattice parameters were set to be $a=5.88$ Å and $c=43.52$ Å (space group: $R\bar{3}m$). The sample with dimensions of about $5 \times 5 \times 4$ mm^3 was fixed on an aluminum plate with aluminum wire and mounted into either 4 K cryocooler or 6 T vertical field cryomagnet for zero and applied magnetic-field experiment, respectively. An incident neutron energy of 14.7 meV was adopted for all of the measurements. For the unpolarized neutron experiments pyrolytic graphite monochromator and analyzer were used and the collimations were chosen as open–40′-40′-80′. Magnetized Heusler monochromator and analyzer were used for the polarized neutron experiments and the collimations were chosen as open–80′-80′-80′. A vertical guide field along the beam path was applied to maintain the polarization of the incident and scattered neutron beam. The polarized neutron experiments were performed in the field range of 0.5–4.5 T, where the beam polarization was determined to be better than 90% by checking the flipping ratios on fundamental nuclear Bragg peaks. At 4.5 T, a small depolarization (~70%) was observed, probably due to the perturbation of the guide field by the applied B.

III. RESULTS AND DISCUSSION

A. Neutron diffraction at zero magnetic field

For the confirmation of the longitudinal-conical spin state below about 50 K, which was suggested by the observation of the ferromagnetic moment along [001] [see also Fig. 3(a)],[10] we measured neutron diffraction patterns along the $(2\ \bar{2}\ L)$ and $(0\ 0\ L)$ directions at zero magnetic field. As shown in Figs. 2(a) and 2(b), magnetic satellite peaks originating from the helical-spin structure were observed below 200 K at $(2\ \bar{2}\ 1 \pm \delta)$ and $(0\ 0\ 18 \pm \delta)$. As the temperature is decreased, the satellite peaks grow in intensity and the δ value increases up to 0.59 at 12 K. At around 120 and at 12 K, the width of the satellite peaks were the resolution limit as seen in Fig. 2. However, the $(2\ \bar{2}\ 1 \pm \delta)$ peaks show apparent broadening between 70 and 50 K, indicating the presence of two kinds of domains with different magnetic periodicity. Temperature dependence of the integrated intensities of the fundamental peaks and the satellite peaks (estimated by the Gaussian fits) were shown in Figs. 3(b) and 3(c). Since the lattice parameter c is much longer than that of a, the scattering vector $\boldsymbol{Q}$ of $(2, \bar{2}, 1)$ is almost perpendicular to [001]
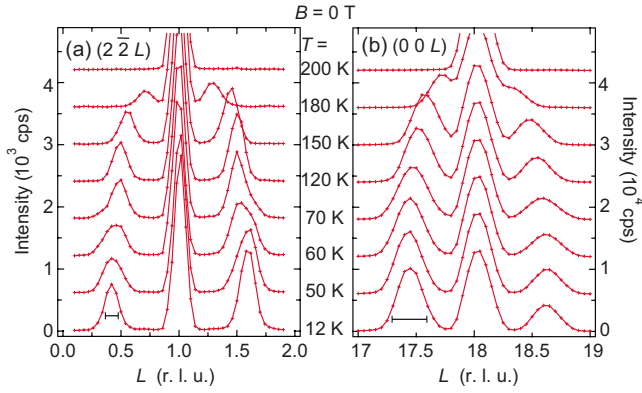
FIG. 2. (Color online) The L-scan profiles of (a) $(2\ \bar{2}\ L)$ and (b) $(0\ 0\ L)$ without external magnetic fields at selected temperatures between 12 and 200 K. The resolutions of the instruments for the $(2\ \bar{2}\ L)$ and $(0\ 0\ L)$ peak profiles are represented by the horizontal bars.

[note that the magnetic scattering cross section is much larger for the satellite peaks of $(2\ \bar{2}\ 1)$ than those of $(3\ \bar{3}\ 0)$]. Thus, the development of the ferromagnetic moment along [001] in the longitudinal-conical spin state below 50 K can be detected as an increase of the $(2\ \bar{2}\ 1)$ reflection intensity, which was indeed observed in Fig. 3(b). This clearly indicates the transition from the proper screw to the longitudinal-conical spin state.

On increasing temperature through 195 K, as the proper-screw phase becomes the collinear ferrimagnetic phase with a ferromagnetic moment lying on the (001) plane, both of the fundamental reflection intensities increase. Because the ferromagnetic moment is absent in the proper-screw phase and the $(2\ \bar{2}\ 1)$ reflection intensity is constant between 50 and 120 K, we assumed that the $(2\ \bar{2}\ 1)$ reflection at 120 K involves only the nuclear Bragg reflection which is constant in all the temperature range. Then the cone angle α below 50 K was estimated by subtracting the intensity of nuclear Bragg reflection from that of the $(2\ \bar{2}\ 1)$ reflection [see Fig. 3(d)]. The α value reaches about 70° at 10 K, giving rise to the ferromagnetic moment of about $2.7\mu_B$ along [001]. For this estimation, we considered the relative magnitude of the L spin moment to the S spin moment, that is 2.8.[22]

Figure 3(d) shows temperature dependence of the turn angle φ determined from the $(2\ \bar{2}\ 1\pm\delta)$ reflections. As temperature decreases below 195 K, φ increases and makes a plateau below 120 down to 50 K, where the helical spins are commensurate as $\delta=0.5$ ($\varphi=60°$), reflecting the magneto-crystalline anisotropy of the hexagonal symmetry. Below about 50 K, the commensurability becomes less favored and φ jumps from 60° to about 70° with exhibiting phase coexistence, which suggests that the transition is of the first order. The reason why the commensurate-incommensurate transition is correlated with the proper-screw to longitudinal-conical transition remains unclear at the present.

B. Neutron diffraction under transverse magnetic fields

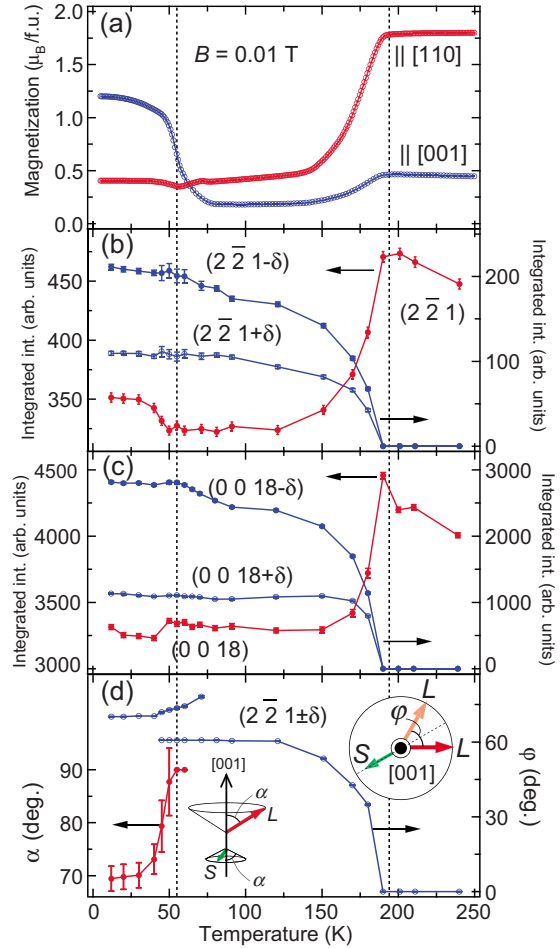Next, we have studied how the helimagnetic structure changes as a function of transverse B at selected tempera-

FIG. 3. (Color online) Temperature dependence of (a) magnetizations parallel to [110] and [001], (b) integrated intensities of the scattering peaks at $(2\ \bar{2}\ 1)$ and $(2\ \bar{2}\ 1\pm\delta)$ and (c) at $(0\ 0\ 18)$ and $(0\ 0\ 18\pm\delta)$, and (d) the cone angle α and the turn angle φ between the adjacent L (or S) spins. The magnetizations were measured under a magnetic field of 0.01 T and the neutron diffraction data were collected without external magnetic field.

tures, or as a function of temperature in fixed B. Based on the results presented in the following, and also taking into account the results in earlier reports,[25,29] a magnetic phase diagram was obtained. As shown in Fig. 1, several phases as characterized by commensurate k_0 appear in B in addition to the incommensurate phase (FE1) which is realized at zero or weak B. Figures 4(a)–4(c) show the L-scan profiles around the fundamental reflections of $(3\ \bar{3}\ 0)$ and $(0\ 0\ 18)$. For all the measurements, B was first set to -0.5 T and then increased up to 1 T with collecting the data at selected B so as to realize the same condition as in the P measurements. At 3.5 K and at low $B \leq 0.3$ T, the satellite peak profiles are severely broadened probably due to the coexistence of two or more helimagnetic phases with different k_0 vectors and thus to the reduced coherence length. This strong hysteretic nature reflects the first-order phase transitions involving commensurate phases and the domain freezing at low temperatures. On the other hand, such broadening is less noticeable for the peak profiles measured at 30 K shown in Fig. 4(b) so that each phase can be easily distinguished. Since the inten-
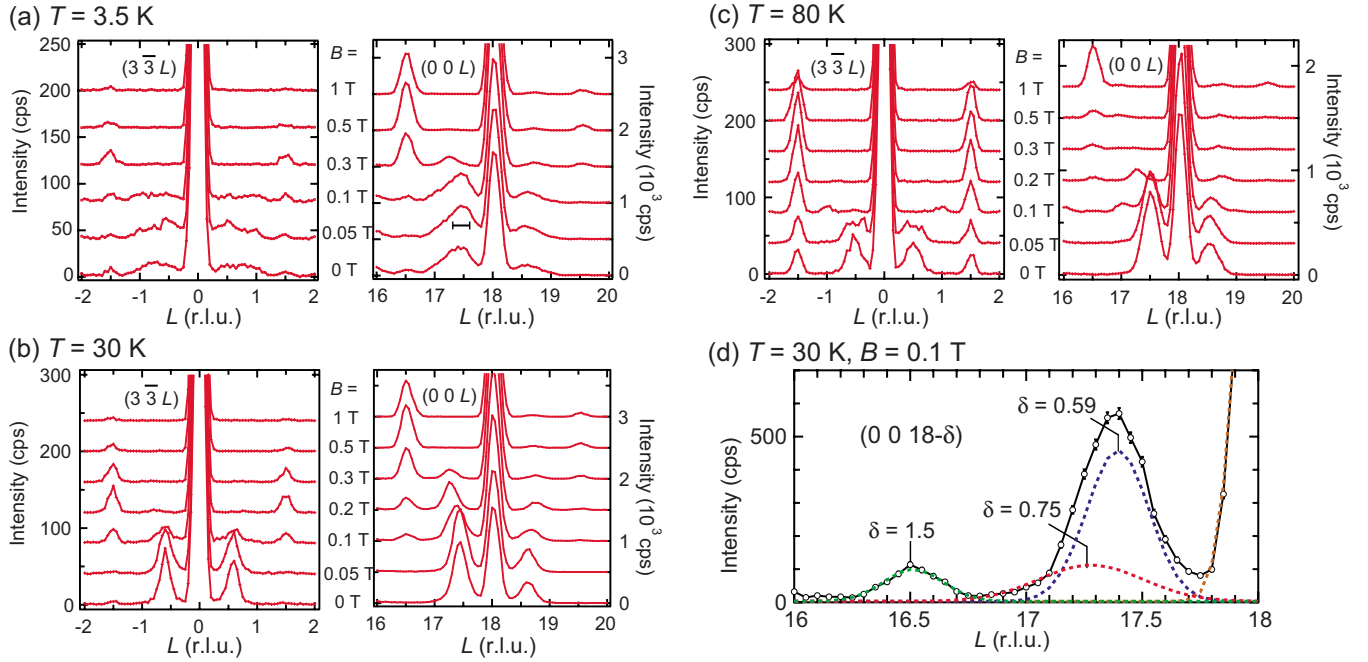
FIG. 4. (Color online) The *L*-scan profiles of (3 $\bar{3}$ *L*) and (0 0 *L*) at (a) 3.5, (b) 30, and (c) 80 K under external magnetic fields *B* along [110]. (d) Magnified view of the *L*-scan profiles of (0 0 *L*) at 30 K and at 0.1 T with highlighting the multiple Gaussian fits. The resolution of the instruments for the (0 0 *L*) peak profile is represented by the horizontal bar in the right panel of (a).

sities of the incommensurate satellite peaks at $\delta \sim 0.59$ remain almost the same upon increasing *B* from 0 to 0.05 T, the phase at around 0.05 T (FE1) was assigned to be slanted longitudinal-conical phase, whose screw axis is deviated from [001] to the direction of *B* (see the upper panel of Fig. 1). Therefore, the *P* reversal by the low-*B* of ± 30 mT at 5 K as demonstrated in a previous study[10] can be explained by the swing of the cone axis with conserving the spin helicity. In Fig. 4(b), at 30 K and above 0.1 T, one can find two kinds of commensurate satellite peaks with $\delta = 0.75$ and $\delta = 1.5$ as has been reported in Ref. 25. While the satellite peak at $\delta = 0.75$ was assigned to be the FE2′ phase, the other peak at $\delta = 1.5$ involves two kinds of phases, FE2 and FE3. At 80 K, another commensurate magnetic phase with $\delta = 1$, named FE1′, was barely observed at 0.1 T as shown in Fig. 4(c). It should be noted that at 80 K the (3 $\bar{3}$ 0 $- \delta$) reflections with $\delta = 1.5$ exists even at 0 T, indicating the presence of FE2 phase as a minority phase. Once a ferromagnetic domain was formed by the application of transverse *B*, it tends to remain robustly even after the removal of *B*.

As the sixfold periodicity [$k_0 = (0, 0, 1/2)$] was found for the proper-screw phase between 50 and 120 K at zero field, the threefold periodicity [$k_0 = (0, 0, 1)$] for the FE1′ phase reminds us of the hexagonal symmetry of the Y-type hexaferrite structure. Thus, it is likely that the screw axis of the FE1′ phase is close to [001] as well as the proper-screw phase. On the other hand, provided that the FE2′, FE2, and FE3 phases have a spin spiral structure, it is reasonable to presume that the screw axes of them are parallel to *B* (∥[110]) because the fourfold [$k_0 = (0, 0, 3/4)$] or twofold periodicity [$k_0 = (0, 0, 3/2)$] can be better viewed as reflecting the twofold rotational symmetry around the [110] direction rather than the hexagonal symmetry around the [001] direction.

The integrated intensities of the satellite reflections and the fundamental reflections as a function of the transverse *B* were plotted in Fig. 5. The fits were done using multiple Gaussian functions, as shown in Fig. 4(d). However, as for the peak profiles at 3.5 K, the fits were reliable only for $\delta = 1.5$ because the other satellite reflections at around $\delta = 0.59$ were overlapping and severely broadened. The δ values for the commensurate magnetic phases such as $\delta = 0.75$, 1, and 1.5 were fixed during the refinements. Since the (3 $\bar{3}$ 0) reflection and the (0 0 18) reflection detect the magnetic moments on the (1 $\bar{1}$ 0) plane and the (0 0 1) plane, respectively [see Fig. 8(a)], the increase in both the fundamental reflection intensities by application of *B* (∥[110]) shown in Fig. 5 indicates the development of the ferromagnetic moment along *B*. When taking a look at the magnetization curves of 5 and 30 K in Fig. 5(a), stepwise changes can be found at around 0.1 and 0.25 T, indicating the *B*-induced phase transitions. Field dependence of the intensity of each satellite peak shown in Figs. 5(b) and 5(c) clearly indicates that the FE1 phase tends to be diminished, and both the FE2 and FE2′ phases emerge at around 0.1 T, where *P* at 5 K and the magnetization at 5 and 30 K increase drastically. This behavior can be regarded as the transition from the slanted longitudinal-conical phase with low *P* of about 20 μC/m^2 to the transverse-conical phases with large *P* of about 80 μC/m^2. The stepwise change in the magnetization curve at around 0.25 T corresponds to the transition between the FE2 and the FE3 phases with the same k_0 vector of (0, 0, 3/2). Upon the transition from the FE2 to the FE3 phase, the reflection intensity of (3 $\bar{3}$ 0 $\pm \delta$) decreases, whereas that of (0 0 18 $\pm \delta$) increases, which should reflect the reorientation of spins as will be discussed later. The transition between them can be more clearly seen at around 0.5 T
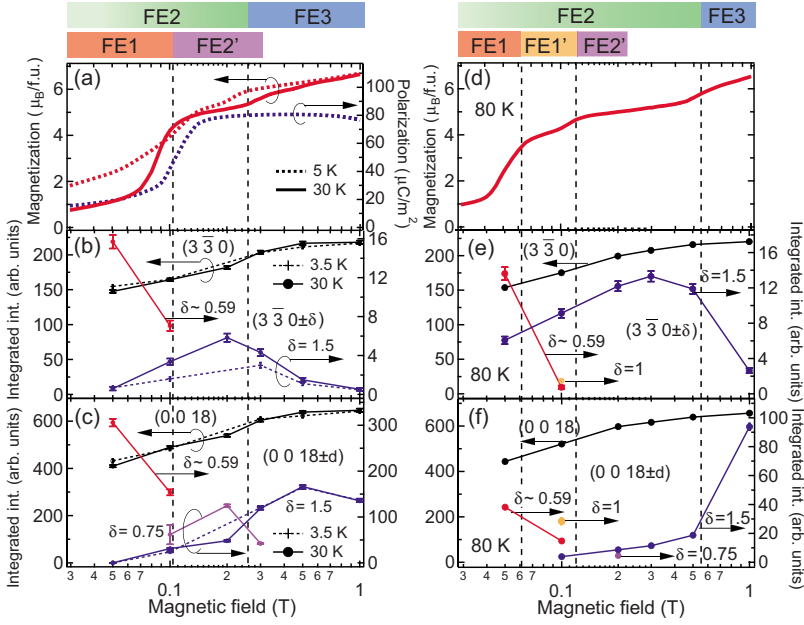
FIG. 5. (Color online) Magnetic-field dependence of (a) magnetizations, (b) integrated intensities of the scattering peaks at $(3\ \bar{3}\ 0)$ and $(3\ \bar{3}\ 0 \pm \delta)$, and (c) at $(0\ 0\ 18)$ and $(0\ 0\ 18 \pm \delta)$ taken at 3.5 (broken lines) and 30 K (solid lines). Magnetic field is applied parallel to [110]. The polarization data taken at 5 K are also shown in (a). Magnetic-field dependence of (d) magnetization, (e) integrated intensities of the scattering peaks at $(3\ \bar{3}\ 0)$ and $(3\ \bar{3}\ 0 \pm \delta)$, and (f) at $(0\ 0\ 18)$ and $(0\ 0\ 18 \pm \delta)$ taken at 80 K. Above the panels, stable regions of each phase are shown as a function of magnetic field, indicating the phase coexistence.

in the data set taken at 80 K [see Figs. 5(e) and 5(f)]. At 80 K, the presence of the FE1′ phase at around 0.1 T gives rise to a plateau in the magnetization curve [see Fig. 5(d)]. On the other hand, the presence of the FE2′ phases seems to be less effective on the magnetization curves.

Figure 6 shows the L-scan profiles of $(3\ \bar{3}\ L)$ and $(0\ 0\ L)$ under a transverse $B\ (\parallel [110])$ of 0.5 T at several temperatures. The reflection intensities of $(3\ \bar{3}\ 0 \pm \delta)$ and $(0\ 0\ 18 \pm \delta)$ with $\delta = 1.5$ change in the opposite way in the range between 90 and 50 K; $(3\ \bar{3}\ 0 \pm \delta)$ decreases in intensity, while $(0\ 0\ 18 \pm \delta)$ increases, as temperature is reduced. This behavior is clearly seen in Figs. 7(b) and 7(c), suggesting the gradual reorientation of spins during the transition from the high-temperature FE2 phase to the low-temperature FE3 phase. As shown in Fig. 7(a), on decreasing temperature, the magnetization measured under transverse B of 0.5 T decreases as the high-temperature collinear phase becomes the FE2 phase and then increases as the FE3 phase develops. All the observed phases with different periodicity were summarized in Fig. 1 with considering the phase coexistence at low B regions below 0.5 T.
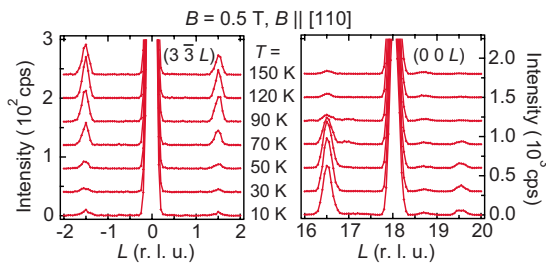
C. Polarized neutron diffraction under transverse magnetic fields

In order to confirm that the FE3 phase with the largest P value has the transverse-conical spin structure instead of the fanlike spin structure, we adopted a polarized neutron diffraction technique. Figure 8(a) describes a couple of experi-
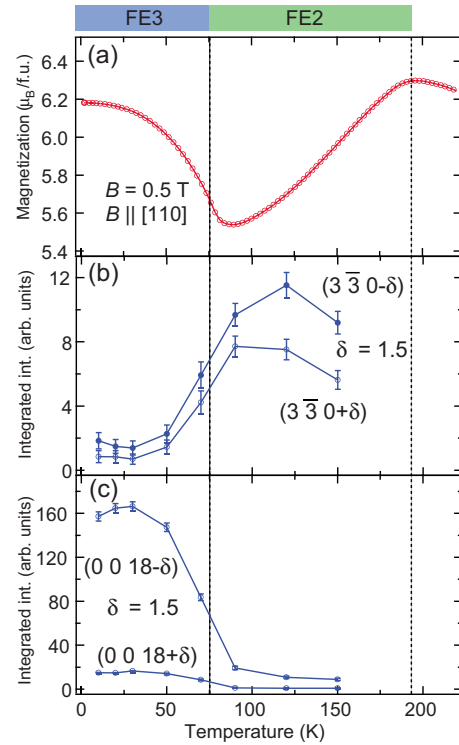

FIG. 6. (Color online) The L-scan profiles of $(3\ \bar{3}\ L)$ and $(0\ 0\ L)$ under a transverse magnetic field $(B \parallel [110])$ of 0.5 T at selected temperatures between 10 and 150 K. A small peak at $(0\ 0\ 18.7)$ comes from the diffraction of aluminum of the sample holder. The ratio between $(3\ \bar{3}\ 0 \pm \delta)$ and $(0\ 0\ 18 \pm \delta)$ reflection intensities largely changes at around 80 K.

FIG. 7. (Color online) Temperature dependence of (a) magnetization parallel to [110], (b) integrated intensities of the commensurate scattering peaks at $(3\ \bar{3}\ 0 \pm \delta)$ and (c) at $(0\ 0\ 18 \pm \delta)$ with $\delta = 1.5$. All the measurements were done under an external magnetic field of 0.5 T applied parallel to [110].
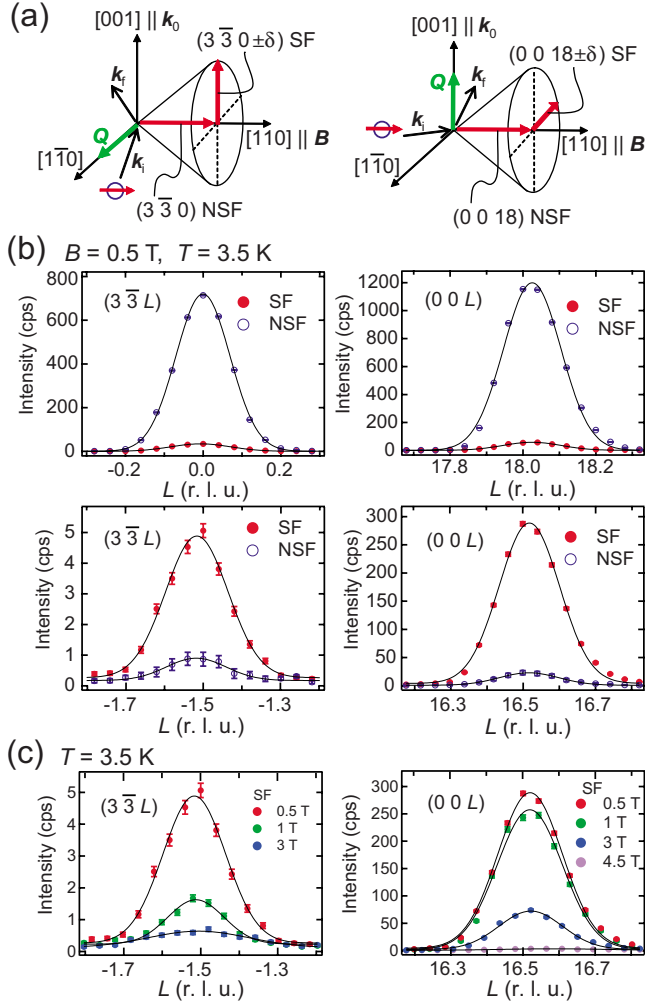
FIG. 8. (Color online) (a) Experimental-setup schematics illustrating the crystal axes of the sample, the scattering vector Q, the magnetic propagation vector k_0 ($\parallel$[001]), the applied magnetic field B ($\parallel$[110]), and the spin direction of the incident polarized neutron ($\parallel$[110]). The ferromagnetic and the helicoidal spin components in the transverse-conical spin state are also shown. (b) L-scan profiles of the fundamental and satellite peaks for $(3\ \bar{3}\ L)$ and $(0\ 0\ L)$ taken at 3.5 K under an applied magnetic field of 0.5 T and (c) various magnetic fields up to 4.5 T. SF and NSF stand for spin-flip and non- spin-flip scatterings, respectively. The solid lines are Gaussian fitting profiles.

mental configurations for the scattering vector Q of $(3,\ \bar{3},\ L)$ and $(0,\ 0,\ L)$. Here, the expected transverse-conical spins propagating along [001] are represented as a single cone for simplicity (but should be regarded as representing the FE3 structure shown in the upper panel of Fig. 1), and are divided into the ferromagnetic component along [110] ($\parallel B$) and the helimagnetic component normal to [110], the latter of which is further divided into the [001] and [1$\bar{1}$0] components. Given the ferromagnetic moment along [110], which is parallel to the spin of the incident polarized neutrons, only the non-spin-flip (NSF) channel gives magnetic scattering intensity at the fundamental reflections. On the other hand, since the helimagnetic components are parallel to [001] and [1$\bar{1}$0], and perpendicular to the spin of the polar-

ized neutrons, only the spin-flip (SF) channel gives the scattering intensity at $(3\ \bar{3}\ 0\pm\delta)$ and $(0\ 0\ 18\pm\delta)$, respectively.

First, at 3.5 K and at 0.5 T, the NSF channel gives strong scattering intensity for the fundamental reflections of $(3\ \bar{3}\ 0)$ and $(0\ 0\ 18)$, whereas the SF channel does much less scattering intensity for them, as shown in the upper panels of Fig. 8(b). This result is consistent with either the transverse-conical spin structure or the fanlike spin structure because both of them carry ferromagnetic moments parallel to [110] (note that the NSF channel involves the nuclear scattering as well as the magnetic scattering). Then, these spin structures can be distinguished by checking the SF channel for Q of $(3,\ \bar{3},\ L)$ sensitive to the [001] component of spins. In the case of the fanlike spin structure, all the spins are lying on the (0 0 1) plane, giving rise to the scattering intensity for the SF channel at $(0\ 0\ 18\pm\delta)$ but not for the SF channel at $(3\ \bar{3}\ 0\pm\delta)$. As seen in the lower panels of Fig. 8(b), the strong scattering intensity can be found for the SF channel of the commensurate satellite peaks, evidencing the presence of the helical-spin components out of and within the (001) plane, respectively. Because the L and the S spins are stacking alternatively along [001] with k_0 of (0, 0, 3/2), we conclude that the FE3 phase has a transverse-conical spin structure, in which the projected spin on the (1 1 0) plane shows a 90° rotation in going from the L block to the adjacent S block (see Fig. 1).

Provided that the planar magnetic anisotropy is very weak, there are twofold degenerate states for the transverse-conical phase with k_0 of (0, 0, 3/2), one with the L spins lying on the (001) plane and the other with the L spins out of the (001) plane. It was shown in Figs. 5 and 7 that the reflection intensity of $(3\ \bar{3}\ 0\pm\delta)$ decreases and that of $(0\ 0\ 18\pm\delta)$ increases drastically as the phase changes from FE2 to FE3, indicating that [001] and [1$\bar{1}$0] component of the helical spins decreases and increases, respectively, upon this transition. Therefore, we have assigned the FE3 phase as having the L spins lying on the (001) plane and the S spins lying on the (1$\bar{1}$0) plane, and the FE2 phase as vice versa. The transition between them can be described as a spin reorientation with rotating the helical component of spins by 90° around [110] direction and thus preserving the spin helicity.

Figure 8(c) shows the intensity of the satellite peaks at selected B ($\parallel$[110]) up to 4.5 T; at the maximum B of 4.5 T the reflection intensity for (0 0 16.5) is zero and the ferroelectricity disappears. By application of the transverse B, the longitudinal-conical spin structure at 0 T changes into the transverse conical. Further application of B squeezes the transverse cone, and eventually drives the cone into the collinear ferrimagnetic structure, being consistent with the P measurements shown in Fig. 9. On the basis of the spin-current model with using the satellite reflection intensities shown in Fig. 8(c), we have calculated B dependence of P in the FE3 phase. With the use of the magnetic form factor for the Fe^{3+} ions, the integrated intensities of the satellite peaks at $(3\ \bar{3}\ 1.5)$ and at (0 0 16.5) were normalized, providing the [001] component arising from the S spins, $S^{[001]}$, and the
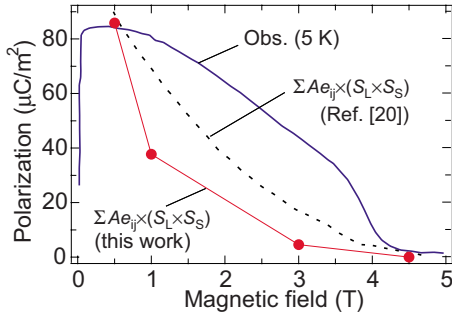
FIG. 9. (Color online) Magnetic-field (along [110]) dependence of electric polarization in the FE3 phase of $Ba_2Mg_2Fe_{12}O_{22}$ at 5 K together with the calculated polarizations based on the polarized neutron diffraction data (solid circles) and the magnetization data (a broken line, Ref. 20) with adopting the spin-current mechanism.

IV. SUMMARY

In summary, we have reported extensive neutron diffraction experiments proving the existence of the longitudinal-conical spin phase at zero field and the several transverse-conical spin phases with commensurate k_0 vectors under transverse B. The presence of the longitudinal-conical spin phase below 50 K, which is adiabatically connected to the slanted conical phase (FE1) with a finite P, can be associated with the low-B control of P (Refs. 10 and 11) as well as the gigantic magnetochromism at terahertz frequencies.[24] In addition, the magnetic phase diagram providing the relation between the magnetic structure and the magnetoelectric property of each phase has been investigated by analyzing the neutron diffraction data with considering the magnetization and the electric-polarization data. Due to the strong hysteresis arising from the first-order nature of the B-induced transitions and the ferromagnetic nature of all the phases except for the proper-screw phase, two or even more phases are coexisting at low B below 0.5 T. By using the polarized neutron diffraction technique, we have verified that the FE3 phase with the largest P with $k_0 = (0, 0, 3/2)$ has a transverse-conical spin structure in which the spin component perpendicular to B shows every 90° rotation with translation along the [001] direction. Although the spin-current model did not quantitatively reproduce the B dependence of the observed P, the overall features such as the negative slope of P and the disappearance of P in the collinear ferrimagnetic phase at 4.5 T have been well described by this model. We believe that our results would be informative also for discussing the magnetoelectric properties of other Y-type hexaferrites with a helimagnetic ground state such as $Ba_{0.5}Sr_{1.5}Zn_2Fe_{12}O_{22}$ (Refs. 9, 29, and 30).

[1̄10] component arising from the L spins, $S^{[1\bar{1}0]}$, in an arbitrary unit. Assuming that the coupling constant A is independent of B in the FE3 phase, the calculated polarization P_{calc} in an arbitrary unit is proportional to $|S^{[1\bar{1}0]} \times S^{[001]}|$. As shown in Fig. 9, although the general trend of P_{calc} as a function of B was similar to the observed P, P_{calc} did not quantitatively reproduce the B dependence of the observed P. Such discrepancy has been discussed for the calculated polarization based on the magnetization measurements, by which $S^{[001]}$ and $S^{[1\bar{1}0]}$ were estimated with assuming the same cone angle for L and S spins (see the broken line in Fig. 9).[20] As an origin for the discrepancy, we may have to consider at least two possibilities: the first one is the possibility of the noncollinearity of spins in each L and S block. If the spins in each block are noncollinear, the relative angles of them within each block should change with increasing transverse B so that P_{calc} based on the spin-current model would be subject to significant modification. The second one is the effect of the lattice degrees of freedom on P induced by the helimagnetic order.[16,27,28] The present model is based on the purely electronic origin such as the spin-orbit interaction causing the polarization of the charge density distribution. The lattice displacements, which always occur more or less as accompanied by the magnetic modulation through the exchange striction mechanism, may play an important role in the ferroelectricity, in particular the magnitude of P, of the present system.

*ishiwata@ap.t.u-tokyo.ac.jp

[1] T. Kimura, T. Goto, H. Shintani, K. Ishizaka, T. Arima, and Y. Tokura, Nature (London) **426**, 55 (2003).

[2] G. Lawes, A. B. Harris, T. Kimura, N. Rogado, R. J. Cava, A. Aharony, O. Entin-Wohlman, T. Yildrim, M. Kenzelmann, C. Broholm, and A. P. Ramirez, Phys. Rev. Lett. **95**, 087205 (2005).

[3] M. Kenzelmann, A. B. Harris, S. Jonas, C. Broholm, J. Schefer, S. B. Kim, C. L. Zhang, S.-W. Cheong, O. P. Vajk, and J. W. Lynn, Phys. Rev. Lett. **95**, 087206 (2005).

[4] T. Arima, A. Tokunaga, T. Goto, H. Kimura, Y. Noda, and Y. Tokura, Phys. Rev. Lett. **96**, 097202 (2006).

[5] Y. Tokura, Science **312**, 1481 (2006).

[6] S. W. Cheong and M. Mostovoy, Nature Mater. **6**, 13 (2007).

[7] Y. Yamasaki, H. Sagayama, T. Goto, M. Matsuura, K. Hirota, T. Arima, and Y. Tokura, Phys. Rev. Lett. **98**, 147204 (2007).

[8] Y. Tokura and S. Seki, Adv. Mater. **22**, 1554 (2010).

[9] T. Kimura, G. Lawes, and A. P. Ramirez, Phys. Rev. Lett. **94**, 137201 (2005).

[10] S. Ishiwata, Y. Taguchi, H. Murakawa, Y. Onose, and Y. Tokura,

Science **319**, 1643 (2008).

[11] K. Taniguchi, N. Abe, S. Ohtani, H. Umetsu, and T. Arima, Appl. Phys. Express **1**, 031301 (2008).

[12] Y. S. Chai, S. H. Chun, S. Y. Haam, Y. S. Oh, I. Kim I, and K. H. Kim, New J. Phys. **11**, 073030 (2009).

[13] S. H. Chun, Y. S. Chai, Y. S. Oh, D. Jaiswal-Nagar, S. Y. Haam, I. Kim, B. Lee, D. H. Nam, K.-T. Ko, J. H. Park, J.-H. Chung, and K. H. Kim, Phys. Rev. Lett. **104**, 037204 (2010).

[14] H. Katsura, N. Nagaosa, and A. V. Balatsky, Phys. Rev. Lett. **95**, 057205 (2005).

[15] M. Mostovoy, Phys. Rev. Lett. **96**, 067601 (2006).

[16] I. A. Sergienko and E. Dagotto, Phys. Rev. B **73**, 094434 (2006).

[17] C. Jia, S. Onoda, N. Nagaosa, and J. H. Han, Phys. Rev. B **76**, 144424 (2007).

[18] T. Nagamiya, J. Appl. Phys. **33**, 1029 (1962).

[19] H. Murakawa, Y. Onose, K. Ohgushi, S. Ishiwata, and Y. Tokura, J. Phys. Soc. Jpn. **77**, 043709 (2008).

[20] S. Ishiwata, Y. Taguchi, Y. Tokunaga, H. Murakawa, Y. Onose, and Y. Tokura, Phys. Rev. B **79**, 180408(R) (2009).

[21] J. Smit and H. P. J. Wijn, *Ferrites* (Philips Technical Library, Eindhoven, 1959).

[22] N. Momozawa, Y. Yamaguchi, and M. Mita, J. Phys. Soc. Jpn. **55**, 1350 (1986).

[23] N. Momozawa, Y. Nagao, S. Utsumi, M. Abe, and Y. Yamaguchi, J. Phys. Soc. Jpn. **70**, 2724 (2001).

[24] N. Kida, D. Okuyama, S. Ishiwata, Y. Taguchi, R. Shimano, K. Iwasa, T. Arima, and Y. Tokura, Phys. Rev. B **80**, 220406(R) (2009).

[25] H. Sagayama, K. Taniguchi, N. Abe, T. H. Arima, Y. Nishikawa, S. I. Yano, Y. Kousaka, J. Akimitsu, M. Matsuura, and K. Hirota, Phys. Rev. B **80**, 180419(R) (2009).

[26] M. Takeda, M. Nakamura, K. Kakurai, E. Lelièvre-berna, F. Tasset, and L.-P. Regnault, Physica B **356**, 136 (2005).

[27] A. Malashevich and D. Vanderbilt, Phys. Rev. Lett. **101**, 037210 (2008).

[28] H. J. Xiang, S.-H. Wei, M.-H. Whangbo, and J. L. F. Da Silva, Phys. Rev. Lett. **101**, 037209 (2008).

[29] N. Momozawa and Y. Yamaguchi, J. Phys. Soc. Jpn. **62**, 1292 (1993).

[30] P. Novák, K. Knížek, and J. Rusz, Phys. Rev. B **76**, 024432 (2007).